Computers in Biology and Medicine 106 (2019) 46–53

Contents lists available at ScienceDirect

Computers in Biology and Medicine

journal homepage: www.elsevier.com/locate/compbiomed

Effects of left atrium on intraventricular flow in numerical simulations

Boyang Su[a,*], Xikun Wang[b], Foad Kabinejadian[c], Calvin Chin[a,d], Thu Thao Le[a,d], Jun-Mei Zhang[a,d]

[a] National Heart Research Institute Singapore, Singapore
[b] Research Center of Fluid Machinery Engineering and Technology, Jiangsu University, Zhenjiang, China
[c] Department of Biomedical Engineering, Tulane University, New Orleans, LA, USA
[d] Duke-NUS Medical School Singapore, Singapore

ARTICLE INFO

Keywords:
Left atrium
Computational fluid dynamics
Mitral valve

ABSTRACT

With the aid of cardiac imaging techniques, recent numerical simulations of left ventricular flow can be patient-specific to better mimic physiological conditions. However, studies with a dynamic mitral valve (MV) remain extremely limited. Even so, the left atrium (LA) is usually simplified to be tubular regardless of its complex structure. Studies on the effect of this simplification are limited and observations are controversial. In this study, both tubular and generic atriums were incorporated in patient-specific simulations with and without the MV to qualitatively and quantitatively estimate the effects of the atrial model on downstream ventricular flow. The patient-specific model was generated based on cardiac magnetic resonance (CMR) images of a healthy volunteer, and the dynamic motion of the MV was defined by the contours acquired along long-axis images. Based on the simulations, the influence of the atrial vortices on ventricular flow was significant in the valveless models in terms of flow structure, kinetic energy (KE) and circulation. Although these effects were suppressed in the presence of the MV, the atrial vortices that survived the passage were not trivial, which was evidenced by reduced strength of circulation and undesired flow pattern in the apical region. The flow structure in the generic atrium also dominated the development of ventricular flow in the valveless model. After the MV was incorporated, its effects on the downstream ventricular flow were considerably reduced but not eliminated. Therefore, a proper modelling of atrial flow is necessary, especially for subjects with high ejection fraction (EF).

1. Introduction

Over the decades, various numerical studies have been conducted to understand the potential correlation between left intraventricular flow and cardiac function. Aiming to have a better understanding of intraventricular haemodynamics [1,2], an idealised left ventricle (LV) (e.g., truncated prolate spheroid) was initially modelled without the left atrium (LA), and the mitral valve (MV) was simplified as an orifice. Advancements in imaging techniques have since enabled numerical simulations of patient-specific studies and most simulations focused on healthy left hearts [3–6].

Owing to the complexity of the LA, its reconstruction from routine CMR scans with large spacing has been challenging [7]. In addition, the intraventricular flow is sensitive to the inlet boundary condition (i.e., atrial flow), and unrealistic flow patterns could appear when the physiological LA is incorporated without the MV [3,8]. As a remedy, a tube-shaped LA is widely adopted in CMR-based numerical studies with a uniform or zero normal gradient condition applied at the inlet [9–12]. Indeed, computational studies with the physiological LA and its effect on intraventricular flow are also very limited [5,13–20].

The primary objective of this paper is to analyse the effects of the LA on downstream intraventricular flow under various configurations, as the relevant studies remain very limited and typically have controversial observations [14,21]. In this study, the numerical model included the LA, dynamic MV and LV. In addition to a widely adopted tubular LA, a generic one based on a CT scan was employed. Both MV and LV models were patient-specific and reconstructed from a CMR scan. An arbitrary Lagrangian–Eulerian (ALE) formulation of the Navier–Stokes equations was also used to solve the blood flow in deforming fluid domains, and detailed vortex structures and flow patterns were analysed to quantify these effects.

2. Methods

CMR images of the LV were acquired from a healthy volunteer with written informed consent. The study was then conducted in accordance with the Declaration of Helsinki and later approved by the SingHealth Centralised Institutional Review Board. The scanner used was a Philips

* Corresponding author. 5 Hospital Dr, 169609, Singapore.
E-mail address: bysuntu@gmail.com (B. Su).

https://doi.org/10.1016/j.compbiomed.2019.01.011
Received 25 September 2018; Received in revised form 15 January 2019; Accepted 15 January 2019

Table 1
Voxel sizes in different views.

Views	Short-Axis	Two chamber	Three chamber	Four chamber
Voxel size (mm^3)	0.9375 × 0.9375 × 8	0.875 × 0.875 × 8	1.166 × 1.166 × 8	1.25 × 1.25 × 8

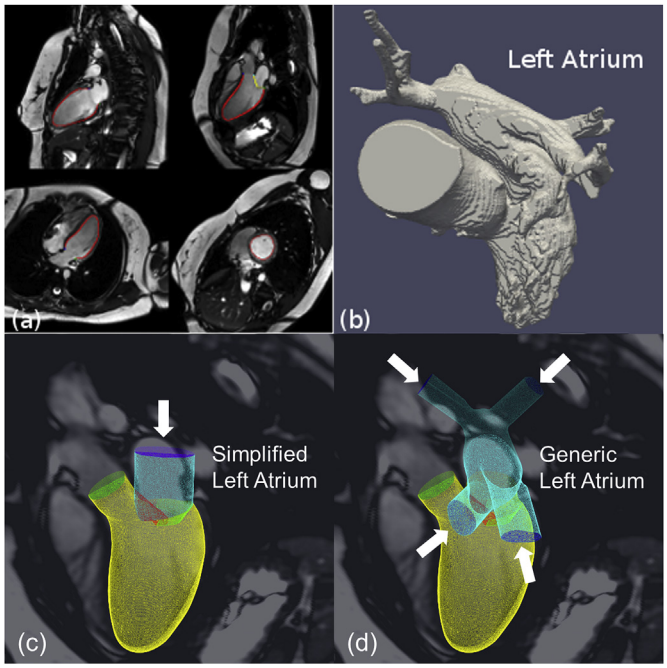

Fig. 1. Reconstruction of left heart model. (a) CMR images in long-axis and short-axis views with manual segmentation. (b) CT-based left heart model from OsiriX database. (c) Reconstructed left heart model with tubular LA. (d) Reconstructed left heart model with generic LA from CT scan. Green: LA; Yellow: LV; Red: anterior leaflet; and White: posterior leaflet. Detailed procedure is available in Ref. [6]. Inlets are indicated by arrows.

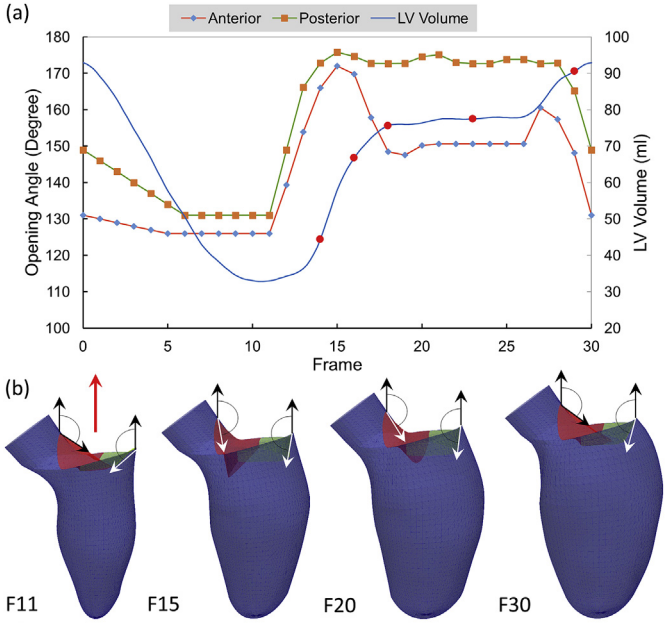

Fig. 2. Geometric information of left heart model. (a) Plots of ventricular volume and leaflet opening angles. (b) Motions of the LV and MV with the opening angle labelled at different frames at the end of systole (Frame 11), rapid filling (Frame 15), diastasis (Frame 20) and at the end of diastole (Frame 30). Red arrow denotes the reference direction.

Ingenia 3.0T MR system (Philips Healthcare; Best, the Netherlands) with a dStream Torso coil (with a maximum number of 32 channels), and balanced steady-state free precession cines were acquired in multiplanar views. Electrocardiography-gated consecutive cine short-axis images were obtained from the apex to the mid-atrium (8 mm slice thickness with 2 mm interslice gap), and the voxel sizes in different views are listed in Table 1. Further, the acquisition rate was 30 frames for each cardiac cycle, with all Digital Imaging and Communications in Medicine (DICOM) images subsequently anonymised before analyses. Manual segmentation was also conducted to delineate endocardium (Fig. 1a), and the spatial information (i.e., resolution, spacing and orientation) enabled the assembly of three-dimensional (3D) contours. The MV was only clearly visible along a three-chamber view, but it crossed other long-axis images. Its generation has been discussed in the supplementary material.

The MV dimensions were also fixed throughout the simulation, yet its relative position to the apex varied. According to the segmentations, the leaflets were moving during the simulation. The dimensions of an average MV during diastole were 25.2 mm × 16.0 mm, and the effective opening area was 322 mm^2 along the long axis, with an effective diameter of 20 mm. Conversely, the diameter of an average LV during diastole was about 40 mm; thus, the ratio of opening area to LV diameter was around 0.5 within the range of 0.44–0.62, as stated by Dahl and Vierendeels [22]. The same topology was applied to each frame, so the resultant surface grids had an identical number of elements and connectivity in STereoLithography (STL) format. An in-house program has been developed to generate the LV from MRI scans using C++ (based on Eigen, Fast Light Toolkit, Grassroots DICOM, the Visualization Toolkit and OpenGL), while the LA was based on a CT scan in the OsiriX database, with ITK-SNAP employed for its segmentation (Fig. 1b). Further, the LA in this study was static without atrial contractions throughout the simulation. The primary purpose of introducing the generic LA was not to mimic the physiological atrial flow that needs additional effects to impose dynamic atrial deformation and inflows from pulmonary veins. Instead, its purpose was to generate complex atrial vortices to demonstrate whether they could survive the passage through the MV. The simplified LA was extruded from the mitral orifice in a tubular shape with a single inlet (Fig. 1c), while the LA based on CT imagery was considered as a generic model with left and right pulmonary veins (Fig. 1d).

Fig. 2a shows plots of LV volume and opening angles at these 30 frames. Volumes at the end of diastole and systole were 93 ml and 33 ml, respectively. The resultant stroke volume was 60 ml and the ejection fraction (EF) was 64.5 per cent, which is within the typical normal range between 55 and 75 per cent. As demonstrated in Fig. 2a, the cardiac cycle includes four typical phases: systole, rapid filling, diastasis and atrial contraction. In this study, the MV was dynamic and its opening angles varied over the cardiac cycle, as shown in Fig. 2a. The MV opened rapidly near the onset of the rapid filling phase, and partial closure was present at diastasis. The second opening of the MV occurred during the atrial contraction phase before its closure at the end of diastole. The opening angle still varied slightly during systole, yet no regurgitation occurred. This was due to the motion of mitral annulus and a pressure gradient variation across the MV. To illustrate the deformations of the LV and MV, Fig. 2b shows the numerical model at the end of systole (Frame 11), rapid filling (Frame 15), diastasis (Frame 20) and at the end of diastole (Frame 30). According to the temporal resolution of CMR, 30 surface meshes were obtained for each

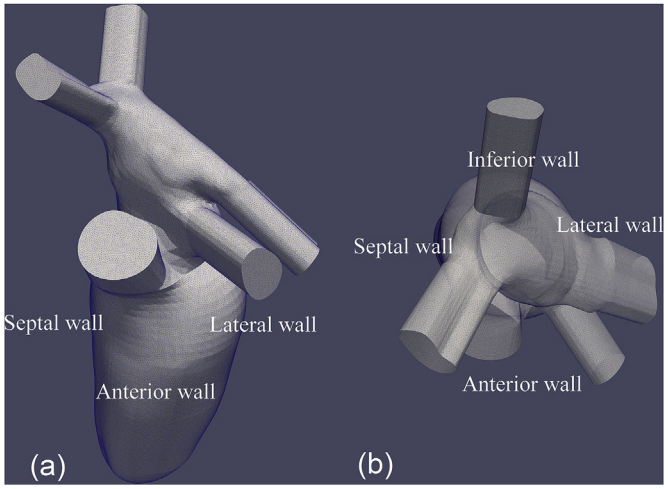

Fig. 3. Numerical model of left heart. (a) Side view (three-chamber view). (b) Top view.

cardiac cycle, which had identical topologies and numbers of nodes. Cubic spline interpolation was also applied to the trajectory of each node on the surface at these 30 key frames to boost the temporal resolution. The duration of one cardiac cycle was 0.861 s (i.e., 70 beats a minute), consisting of 3000 time steps.

In this study, computational fluid dynamics (CFD) software ANSYS FLUENT (Version 16.2) was employed to model blood flow in the left side of the heart, based on the finite volume method in the ALE formulation of the Navier-Stokes equations. Blood flow was assumed to be Newtonian with a constant dynamics viscosity of 3.5 mPa·s and density of 1050 kg/m^3 [23]. Fig. 3 shows a nearly isotropic mesh that was generated using the commercial software ANSYS ICEM CFD. For ease of depiction, four sides of the ventricular wall have been labelled. The spatial resolution was around 0.9 mm and denser grids in the proximity of the MV were generated. The resultant numerical models contained 1.5–2.0 $\times$ 10^6 grids, owing to the different configurations of the LA and MV. The LV and MV were also represented by 4.0 $\times$ 10^4 and 8.2 $\times$ 10^3 triangular surface grids, respectively. Although the total number of volume cells varied with deformation, the number of nodes and their connectivity of the surface grids on the LV and MV must be consistent. To achieve this, the triangular surface grids (CFD) were registered to the surface elements at the first frame, with mapping applied to the remaining frames (detailed information is available in Ref. [24]).

The healthy volunteer did not have noteworthy degrees of regurgitation across the aortic valve or MV, through which the mass flow rate should be close to zero during diastole and systole, respectively. Due to limitations in the dynamic mesh, a narrow clearance gap is needed to maintain a continuous fluid domain; although, the blood in the LA is separated from that in the LV physiologically during systole [22]. As a result, it was challenging to impose a boundary condition at the MV directly. Instead, the inlet of the atrium (i.e., the inlet of the whole numerical model) was set as the wall to maintain a zero flow rate at the MV during systole. Similarly, the outlet of the numerical model (i.e., the aortic orifice) was set to the wall during diastole to mimic the full closure of the aortic valve. Accordingly, the boundary condition at the outlet during systole was pressure outlet at 100 mmHg, and that at the inlet during diastole was pressure inlet at 0 mmHg. No-slip boundary condition was also applied to the walls including the MV, whose motion was prescribed using user-defined functions [6]. The LV movement was derived from CMR images and drove the flow in a unidirectional manner, and a pressure-based solver was selected and a SIMPLEC scheme was employed for the pressure-velocity coupling. The spatial discretisation of pressure and momentum were of second order, while temporal discretisation was only first order; this was recommended when the dynamic mesh module was activated. The numerical simulations lasted for three cardiac cycles and the results presented were based on the last cycle [12,25–27].

It is believed that kinetic energy (KE) is a potential marker of ventricular dysfunction. Its area-averaged value of in-plane flow is defined by:

$$KE = \frac{\int\int_S \frac{1}{2}\rho(u^2 + v^2)ds}{S} \quad (1)$$

where u and v denote the two-dimensional flow velocity, ρ is the fluid density and s is the area. To quantify the circulation motion of the ventricular flow in the three-chamber view, the area integration of vorticity (i.e., circulation, Γ) is defined by:

$$\Gamma = \int\int_s \left(\frac{dv}{dx} - \frac{du}{dy}\right)ds \quad (2)$$

The clockwise direction in the three-chamber view shown in Fig. 1a is defined as positive.

3. Results

3.1. Vortex structures in diastolic flow

Four left heart models with identical LVs have been simulated, and the inside vortex structures will be depicted in this section. The dominant flow pattern during systole is the streaming of small vertical structures out of the LV, and it is not closely related to the characteristics of ventricular flow. As a result, in this and many other studies the focus is on the flow phenomena in diastole [10,22,28–30]. For ease of understanding, the valvular model with a simplified LA (Model A) will be introduced first, in which the flow field is dominantly affected by the MV alone. After that, the flow structures in the valvular model with the generic LA (Model B) will be shown to analyse the combined effects of both the MV and LA. Lastly, the flow fields in two additional valveless models (Models C and D) will be delineated to compare with the corresponding valvular models. The vortex structures shown in this section are at five different time instants: near the onsite of the rapid filling phase (Frame 14), near the end of the rapid filling phase (Frame 16), at the end of the rapid filling phase (Frame 18), at diastasis (Frame 23) and at the time corresponding to atrial contraction (Frame 29), as indicated by '●' in Fig. 2a.

Fig. 4 shows the evolution of the vortex structures in the valvular models (A&B) during diastole, whereby the structures are visualised using the Q-criterion proposed by Dubief and Delcayre [31]. The transvalvular jet resulted in a flow separation at the MV tip rolling up, thus, forming a vortex ring (Fig. 4a). The vortex ring conformed to the geometry of the MV tip and was directed towards the lateral wall by the longer anterior leaflet. The continuous jet further strengthened the vortex ring, manifesting in the enlarged volume even after pinch-off (Fig. 4b). Although the LV expanded in all directions, it was partially exceeded by the growing elliptic vortex ring in the radial direction. As a result, the vortex-wall (i.e., endocardium) interaction resulted in a vortex ring breakdown (Fig. 4b and c). During diastasis, the vortex structure was further disrupted and dissipated (Fig. 4d), and as a result the scattered small-scale vortices were (fairly) uniformly distributed in the LV, except the apical region (Fig. 4d). At the time corresponding to atrial contraction, the second vortex ring could not propagate as deep as the former ring, owing to the short duration of this phase (Fig. 4e). The considerably dilated LV promoted the growth of the second vortex with no obvious disruption observed. Meanwhile, the vortices initiated during the rapid filling phase diminished. In Model B (Fig. 4f–j), the LA flow was much more complex than that in Model A, owing to the collision of vortices generated at the outlets of the pulmonary veins. The ventricular vortex structure was also similar to that in Model A near the onset of the rapid filling phase (Fig. 4f), after which the vortices in the

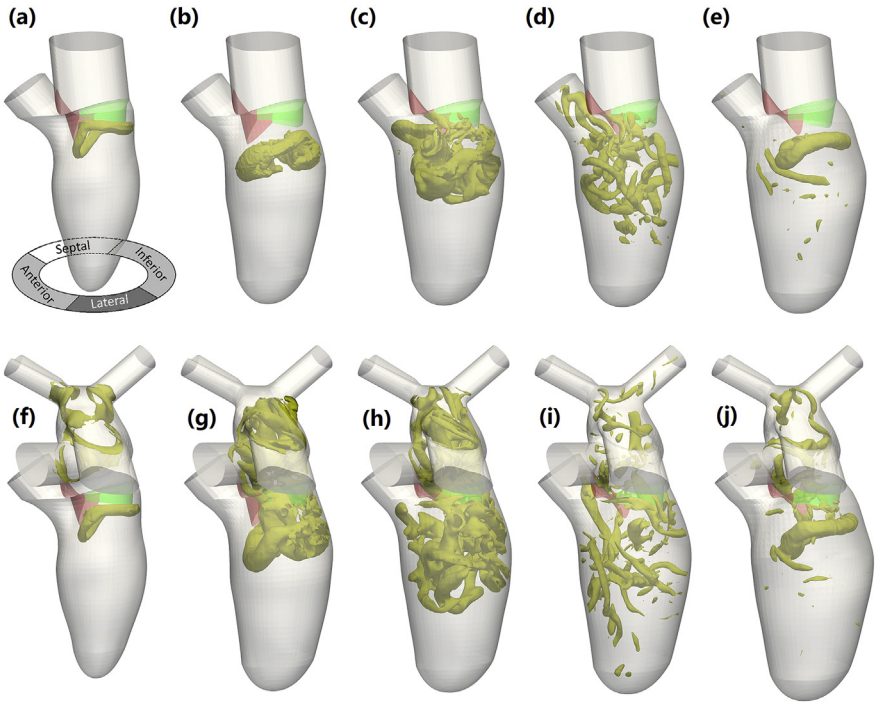

Fig. 4. 3D vortex structure visualised by the isosurface of the Q-criterion vortex identification thresholded at 3000 s^{-2} during diastole in Model A (upper) and B (lower) at five time instants: (a&f) near the onsite of the rapid filling phase (Frame 14), (b&g) near the end of the rapid filling phase (Frame 16), (c&h) at the end of the rapid filling phase (Frame 18), (d&i) at diastasis (Frame 23) and (e&i) at the time corresponding to atrial contraction (Frame 29).

LA were flushed into the LV through the MV (Fig. 4g). Despite the detailed structures, these vortices indicated farther propagation of transvalvular flow towards the apex and enhanced mixing of the LA and LV flows in the generic model (Fig. 4h and i). The second vortex ring formed in the generic model did not differ from Model A significantly, except for the LA vortices (Fig. 4j).

In Model C, the LV was only slightly dilated with respect to the mitral orifice during the early stage of the rapid filling phase. As a result, a flow separation phenomenon was not observed at the anterior, lateral and posterior sides of the LV. The only exception occurred at the root of the outflow tract due to the large divergence curvature at the conjunction of the mitral and aortic roots (Fig. 5a). The vortex ring formed after considerable LV expansion (Fig. 5b) and continued its growth during the rest of the rapid filling phase (Fig. 5c). In addition to the weakened transvalvular jet through the larger mitral orifice, its late occurrence limited the vortex ring's excursion into the core region of the LV (Fig. 5 c&d), compared to the valvular models at corresponding instants (Fig. 4c&d). During the diastasis, the vortex structure largely remained near the mitral orifice and the expanded LV facilitated the flow separation; thus, a weak second vortex ring was observed in the relatively short atrial contraction period (Fig. 5e). Consequently, the presence of a generic LA significantly altered the vortex structure in the LV. The non-uniform transvalvular flow from the generic LA resulted in the generation of a vortex structure in the proximity of the mitral orifice

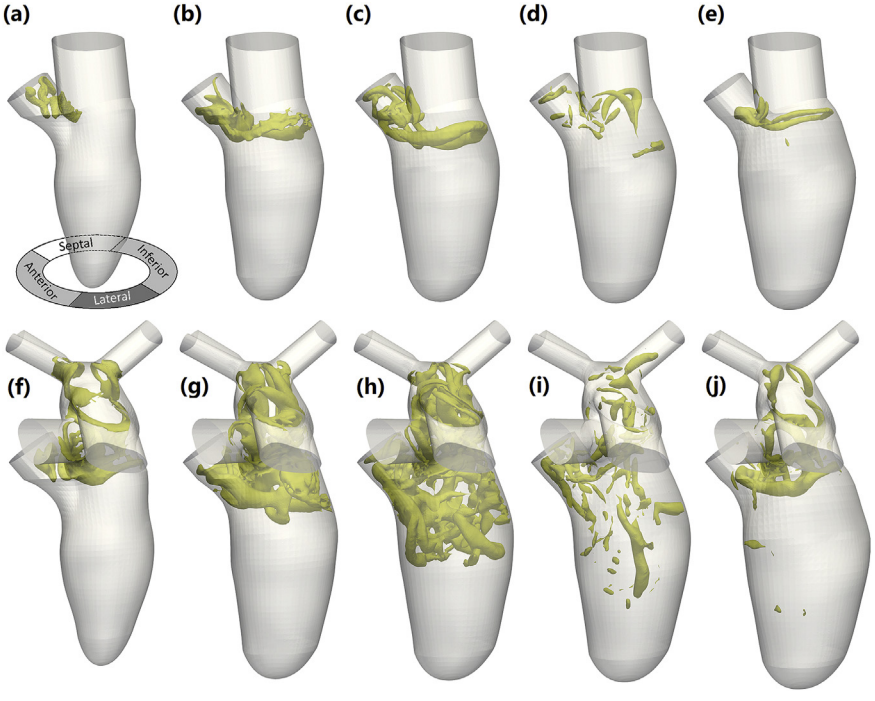

Fig. 5. 3D vortex structure visualised by the isosurface of the Q-criterion vortex identification thresholded at 3000 s^{-2} during diastole in Model C (upper) and D (lower) at five time instants: (a&f) near the onsite of the rapid filling phase (Frame 14), (b&g) near the end of the rapid filling phase (Frame 16), (c&h) at the end of the rapid filling phase (Frame 18), (d&i) at diastasis (Frame 23) and (e&i) at the time corresponding to atrial contraction (Frame 29).

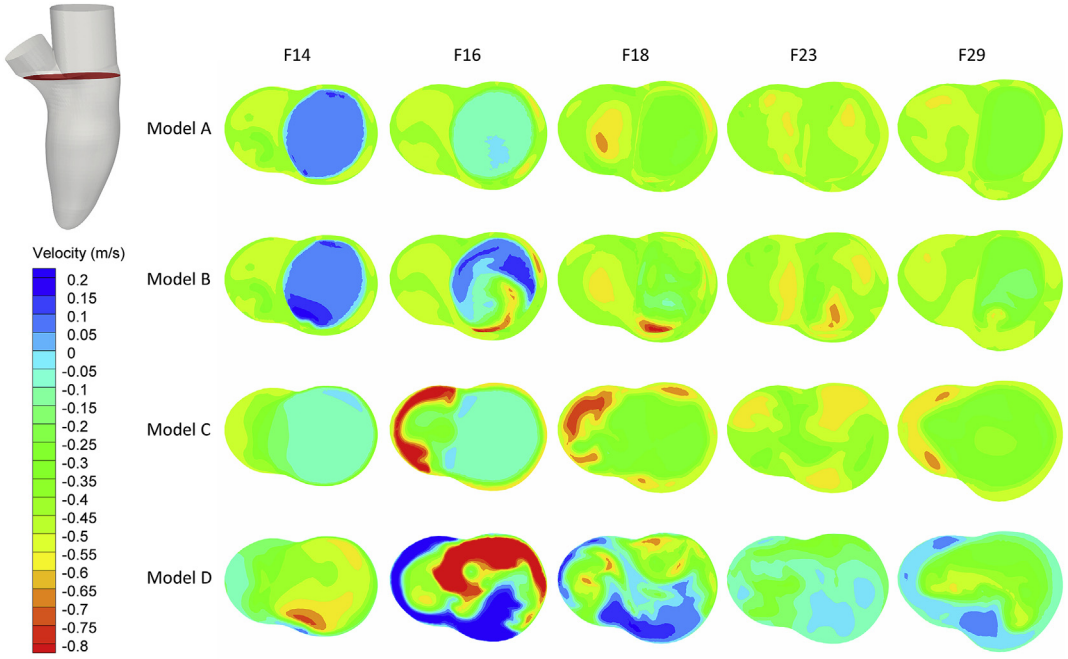

Fig. 6. Contours of transmitral velocity along the long-axis direction in each model at five time instants. Frame 14: near the onsite of the rapid filling phase; Frame 16: near the end of the rapid filling phase; Frame 18: at the end of the rapid filling phase; Frame 23: at diastasis; Frame 29: at the time corresponding to atrial contraction. The plane is perpendicular to the long axis. C. Time-averaged intraventricular flow pattern.

(Fig. 5f), which was not observed in Model C (Fig. 5a). In addition, these vortex structures interacted with those in the LA. With the inflow of blood from the LA, its vortices were subsequently flushed into the LV and overwhelmed the vortex structures generated below the mitral orifice (Fig. 5g). Therefore, no vortex ring was formed during the rapid filling phase in Model D (Fig. 5h). Further, the blood flow from the pulmonary veins was not uniform, and the portion that had high momentum penetrated deeper towards the apex, evidenced by the more uniform and deeply distributed small-scale vortices during diastasis (Fig. 5i). During the atrial contraction phase, its short duration impaired the vortices' influence in the LA on LV flow, and the vortices initiated in the rapid filling phase significantly diminished, regardless of LA configuration (Fig. 5j).

3.2. Transmitral velocity contours during diastole

Alternatively, the effect of the atrial flow can be reflected in the transmitral flow, which is the immediate inlet of intraventricular flow. A cross-sectional view of transmitral flow is selected in the proximity of the mitral orifice, perpendicular to the long axis of the LV, as shown in Fig. 6. Only the flow along the out-of-plane direction (i.e., the long axis) contributes to this transportation. Its contours at the same time instants as Fig. 5 are tabulated for each model.

In Model A, the MV confined transmitral flow, and a clear interface was observed therein during the rapid filling phase (Frames 14 and 16). At stages near the end of rapid filling (Frame 18), diastasis (Frame 23) and atrial contraction (Frame 29), the transmitral flow was much weaker. As a tubular LA was adopted, the transmitral flow was relatively smooth in Model A. In contrast, more obvious variations of transmitral velocity contours were present in Model B, owing to the complex flow structure generated in the LA. This phenomenon is more intense at Frame 16 (Model B) instead of Frame 14 because most of these atrial vortices had yet to reach the MV at Frame 14. As the transmitral flow declined, less atrial vortices streamed into the LV with reduced strength. In Model C, the MV was excluded in the model; thus, the effective opening area was larger, leading to slower transmitral flow even at the rapid filling phase (Frame 14). Again, as the transmitral flow was not regulated by the MV, the flow field near the aortic root was considerably influenced, especially at Frame 16. When the generic LA was employed in the numerical simulation, the transmitral flow became much more complicated, as shown in Model D. Similarly, the largest variation was observed at Frame 16 (Model D) when the complex atrial flow structure entered the LV.

Fig. 7a shows that the in-plane velocity vectors along the three-chamber view are averaged over one cardiac cycle, and the intraventricular region is partitioned into five regions: (1) basal anteroseptal (1), basal inferolateral (2), mid anteroseptal (3), mid inferolateral (4) and the apical region (5); these are based on a cross-section of 17 segmentations along a three-chamber view [32]. As stated by Domenichini and Pedrizzetti [2], the averaged flow field concerns a synthetic description persisting during a cardiac cycle, providing an additional method to analyse ventricular flow. Streamlines are next plotted to indicate the flow direction, and the velocity vectors are scaled by their magnitude. In addition, the Q-criterion contours are superimposed to illustrate vortices or abrupt changes in flow direction. To quantify the flow pattern, the distributions of area-averaged KE and circulation (Γ) in these four models are tabulated in Table 2.

In Model A (Fig. 7b), the high mean velocity at Region 1 was induced by the strong systole flow along the outflow tract, while the one at Region 2 was located between mitral leaflets, which accelerated transvalvular flow. The presence of asymmetric mitral leaflets generated a pair of inclined vortices in the wake, and the tilted transvalvular jet directed the flow to the mid and apical regions in a clockwise direction. As illustrated in Table 2, the KE level reduced significantly from base to apex (by around one order of magnitude) as the flow propagated downwards, owing to energy dissipation and expansion of the LV. Generally, the generic LA did not significantly change the distributions of KE (Table 2) and the velocity vectors (Fig. 7c). For example, the KE level also reduced from base to apex in Model B, and the mean values of KEs in all regions of Models A and B were close to each other (6.08×10^{-3} mJ/cm^3 v. 5.98×10^{-3} mJ/cm^3). Further, the complex flow structure in the generic LA altered the dominant atrial flow in the direction that hindered the formation of clockwise ventricular flow, which is evidenced by the lower circulation from 43.3 cm^2/s in Model A

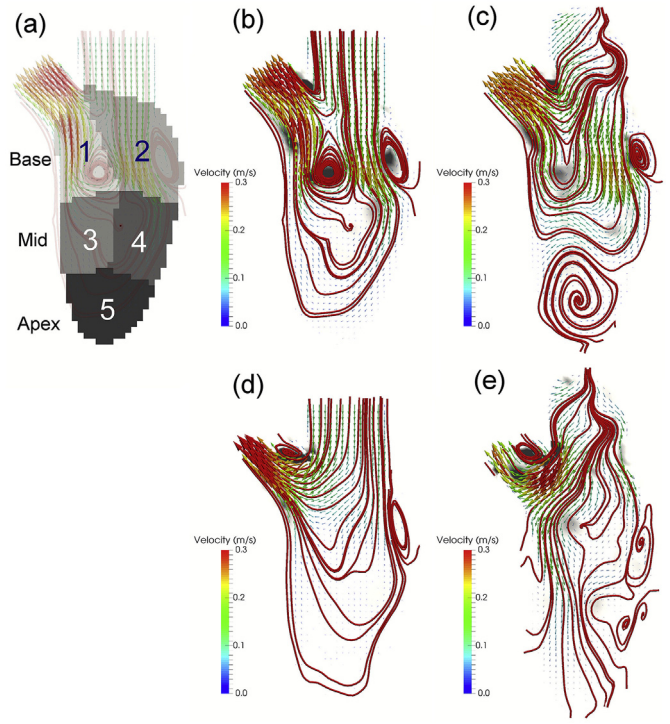

Fig. 7. Time-averaged flow pattern over a cardiac cycle along a three-chamber view. (a) Five partitions and three layers in the LV chamber including basal anteroseptal (1), basal inferolateral (2), mid anteroseptal (3), mid inferolateral (4) and the apical region (5). (b)–(e): Streamlines, velocity vector map and contours of the Q-criterion magnitude in Models A, B, C and D, respectively.

to 27.5 cm^2/s in Model B (Table 2). In addition, the apical flow was counterclockwise, as indicated by the streamlines in Fig. 7b. As shown in Table 2, the KE level in the mid layer (Regions 3 and 4) elevated and that in Region 1 lowered, leading to relatively more uniform KE distribution, which was consistent with the deeper propagation of transvalvular flow and improved mixing of flows observed in Fig. 4h&i.

In the valveless Model C, only Region 1 had high mean velocity, and the abrupt change in flow direction occurred at the aortic root, as indicated by the Q-criterion contours (Fig. 7d). Although a posterior vortex was present, its strength significantly weakened, as indicated by the Q-criterion contours. The KE levels at all regions in Model C also dropped considerably with respect to Model A (2.08×10^{-3} mJ/cm^3 v. 6.08×10^{-3} mJ/cm^3), as well as circulation (13.3 cm^2/s v. 43.3 cm^2/s). Compared to Model C, the generic LA in Model D induced an irregular flow pattern and directed the dominant flow direction counterclockwise, which was indicated by a negative circulation of -20.7 cm^2/s. As such, these irregular vortices escalated the KE level in Model D (3.40×10^{-3} mJ/cm^3 v. 2.08×10^{-3} mJ/cm^3).

4. Discussion

In the present study, four models with identical LVs were simulated to understand the effects of the LA on intraventricular flow with and without the MV. Most of the numerical studies in the literature exclude the MV and have a tubular LA (Model C shown in Fig. 5, upper row). The myocardium near the onset of diastole is hardly dilated with respect to the mitral orifice; thus, the vortex formation is delayed [25,26]. Consequently, the transvalvular flow through the larger mitral orifice has lower momentum, as reflected in the relatively low transmitral flow velocity, leading to shorter propagation into the LV chamber. In some studies, purposely narrowed mitral orifices were adopted as a remedy to facilitate vortex formation and mixing [5,9,10,33]. Indeed, the importance of incorporating MV leaflet dynamics into the flow field in the LV has been analysed in this (Model A) and other recent studies [6,18,20,28]. In a valvular model, the boundary layer separation occurred at the MV tip and the resultant vortex ring was initiated at the onset of the rapid filling phase. In addition, the wake of the MV promoted the growth of the vortex ring in size, which was further propelled towards the apex by a stronger transvalvular flow induced by the smaller, effective opening area of the MV. As listed in Table 2, the mean KE in Model A is about three times higher than that in Model C (6.08×10^{-3} mJ/cm^3 v. 2.08×10^{-3} mJ/cm^3). The asymmetric configuration of the MV also plays an important role in the dominant direction of intraventricular flow, as a longer anterior leaflet directs the flow towards the lateral side of the LV wall, increasing the strength of circulation (43.3 cm^2/s v. 13.3 cm^2/s).

In the valveless model with a generic LA (Model D), its complex structure induced vortices from the onset of the rapid filling phase, while the marginal dilation of the LV with respect to the MV did not allow the generation of a vortex ring, which formed at a later stage. However, the large opening area of the mitral orifice allowed the transportation of these vortices into the LV without much dissipation. Thus, the flow field in the LV was dominated by these vortices, which was consistent with the elevated KE level in Model D compared to Model C. In addition, the generic LA redirected the dominant flow counterclockwise (negative circulation) compared to Model C (-20.7 cm^2/s v. 13.3 cm^2/s). As mentioned by Schenkel et al. [3], solely incorporating a physiological LA without an MV had adverse effect on the numerical simulation of the LV flow; as far as is known, no valveless model in 3D with generic LA is available in the literature. However, a similar, two-dimensional model was investigated by Dahl [20], who observed that the intraventricular flow was not physiological, with no rational flow occurring inside the LV during diastasis in the 2D model with a generic LA and no leaflets. Even if a simplified tubular LA is adopted in the valveless model (Model C), the relative angle of said tubular LA with respect to the LV should be properly defined to avoid the counterclockwise flow direction observed by Seo and Mittal [10], and Pedrizzetti et al. [34].

In the model with the generic LA and dynamic MV (Model B), the atrial vortices underwent higher dissipation when flowing through the MV, which, in turn, influenced intraventricular flow. The

Table 2
Distribution of area-averaged KE in five regions of the LV and circulation in four models (+: Clockwise; −: Counterclockwise).

		Regions in LV					
		1	2	3	4	5	All
Model A	KE (mJ/cm^3)	1.69E-02	8.90E-03	1.10E-03	1.79E-03	3.89E-04	6.08E-03
	Γ (cm^2/s)						+43.3
Model B	KE (mJ/cm^3)	1.21E-02	1.00E-02	2.72E-03	3.34E-03	2.00E-04	5.98E-03
	Γ (cm^2/s)						+27.5
Model C	KE (mJ/cm^3)	6.89E-03	2.86E-03	1.09E-04	7.60E-05	9.14E-06	2.08E-03
	Γ (cm^2/s)						+13.3
Model D	KE (mJ/cm^3)	1.08E-02	4.10E-03	1.80E-03	3.00E-04	1.65E-04	3.40E-03
	Γ (cm^2/s)						−20.7

counterclockwise circulation in Model D ($-20.7\,cm^2/s$) was also restored to a clockwise direction in Model B ($27.5\,cm^2/s$), and the mean KE level increased from $3.4 \times 10^{-3}\,cm^2/s$ to $5.98 \times 10^{-3\,cm2}/s$, respectively. Although Model B was more similar to Model A rather than Model D in terms of vortex structure (Figs. 4 and 5), the discrepancy between these two models demonstrated the influences of the atrial vortices on intraventricular flow structure (Fig. 4), which was further reflected in the reduced circulation ($27.5\,cm^2/s$ v. $43.3\,cm^2/s$).

In the literature, the effect of the physiological LA was qualitatively depicted by Mihalef et al. [21], who mentioned that atrial vortices alter the intraventricular flow insignificantly. Therefore, as they suggested, imposing an appropriate inlet boundary condition that could represent vortices in the physiological LA is a feasible solution in a left heart model with no or simplified LA. Notably, the effects of the LA on intraventricular flow were analysed by Vedula et al. [14] and Lantz et al. [17]. The former group found that most of the vortices in the LA did not survive the passage through the MV, and the effect of the physiological LA was small, with the overall differences limited to about 10 per cent of the peak mitral flow velocity. Similarly, the latter study observed that the effect of LA flow was minor, owing to the regularisation of the MV. Overall, these two studies are consistent with the current one, in that the configuration of the LA did not affect the KE levels in the valvular models ($6.08 \times 10^{-3}\,mJ/cm^3$ in Model A v. $5.98 \times 10^{-3}\,mJ/cm^3$ in Model B). In terms of vortex structures, both studies in the literature agreed that the influence of atrial flow was mild, aligning with the current study. The main discrepancy between these two observations in Refs. [14,21] is whether the transvalvular vorticity transport model is necessary. The present study agreed with the former one in Ref. [21] that the certain vortical transportation model is a reasonable approach to better mimic physiological conditions; this was also observed in the transmitral flow. This is because the survived atrial vortices were able to alter the ventricular flow to some extent, as demonstrated by the undesired apical vortex. In Ref. [14], the EF of the subject was only 43 per cent, which is lower than the normal range of 55–75 per cent (64.5 per cent in the present study). A lower EF induces a lower momentum of blood from the pulmonary veins and weaker vortices, leading to faster dissipation. In addition, the temporal variation of LV volume in Ref. [14] did not include a typical rapid filling phase, diastasis and atrial contraction phases, due to the lower temporal resolution of CT imagery. Evidently, these two limitations both contributed to the discrepancy.

Nevertheless, this study has several limitations. Similar to most numerical studies on LV flow, the effects of the trabeculae and papillary muscles on intraventricular flow were neglected, in part due to the low spatial resolution of the short-axis images in the out-of-plane direction—an intrinsic limitation of routine CMR scans. In the numerical study based on CT imagery with relatively isotropic spatial resolution [14], it has been observed that the trabeculae and papillary muscles considerably altered the vortex structure without significant influence on the overall hydrodynamic efficiency of the ventricle. Second, a generic LA without deformation instead of a patient-specific one was adopted, owing to the incomplete coverage of routine CMR scanning and possibly a desynchronisation of cardiac cycles between different sources (e.g., CMR scan and CT scan). However, as mentioned, the main purpose of introducing the generic LA model was to generate complex atrial vortices. As a result, their passage through the MV and their effects on downstream ventricular flow could be analysed through a comparison with its counterpart with tubular LA. Otherwise, the physiological LA as well as the flow profile within the pulmonary veins must be acquired simultaneously from the same subject. The well-recognised flow pattern was subsequently observed in valvular Model A (Fig. 7b), and the apical vortex in Model B (Fig. 7c) demonstrated the capability of atrial vortices on influencing ventricular flow. Lastly, only single subject was selected under rest condition, meaning the influences of both subject variation and exercise condition were neglected [35].

5. Conclusion

This study found that the atrial vortices only appeared in the generic LA, while the flow in its tubular counterpart was uniform. In the absence of an MV, atrial vortices dominated intraventricular flow, especially during the rapid filling phase, likewise escalating KE levels. Further, the orientation of both tubular and generic atriums must be properly designed to generate clockwise (positive) circulation. After incorporating the MV, the intraventricular flow was less sensitive to the flow pattern in the atrium (i.e., the dominant flow direction was mainly influenced by asymmetric mitral leaflets). However, the influence of a generic LA was not trivial, and the survived atrial vortices could affect the downstream ventricular flow, especially for subjects with high EF. Overall, different observations in the current study and in other relevant studies imply that this framework should be applied to more subjects under various conditions to gain a more comprehensive understanding.

Appendix A. Supplementary data

Supplementary data to this article can be found online at https://doi.org/10.1016/j.compbiomed.2019.01.011.

References

[1] O. Pierrakos, P.P. Vlachos, The effect of vortex formation on left ventricular filling and mitral valve efficiency, J. Biomech. Eng. 128 (2006) 527–539.
[2] F. Domenichini, G. Pedrizzetti, Intraventricular vortex flow changes in the infarcted left ventricle: numerical results in an idealised 3D shape, Comput. Methods Biomech. Biomed. Eng. 14 (2011) 95–101.
[3] T. Schenkel, M. Malve, M. Reik, M. Markl, B. Jung, H. Oertel, MRI-based CFD analysis of flow in a human left ventricle: methodology and application to a healthy heart, Ann. Biomed. Eng. 37 (2009) 503–515.
[4] M.-H. Moosavi, N. Fatouraee, H. Katoozian, A. Pashaei, O. Camara, A.F. Frangi, Numerical simulation of blood flow in the left ventricle and aortic sinus using magnetic resonance imaging and computational fluid dynamics, Comput. Methods Biomech. Biomed. Eng. 17 (2014) 740–749.
[5] C. Chnafa, S. Mendez, F. Nicoud, Image-based simulations show important flow fluctuations in a normal left ventricle: what could be the implications? Ann. Biomed. Eng. (2016) 1–13.
[6] B. Su, R.S. Tan, J.L. Tan, K.W.Q. Guo, J.M. Zhang, S. Leng, X. Zhao, J.C. Allen, L. Zhong, Cardiac MRI based numerical modeling of left ventricular fluid dynamics with mitral valve incorporated, J. Biomech. 49 (2016) 1199–1205.
[7] C.W. Lim, Y. Su, S.Y. Yeo, G.M. Ng, V.T. Nguyen, L. Zhong, R.S. Tan, K.K. Poh, P. Chai, Automatic 4D reconstruction of patient-specific cardiac mesh with 1-to-1 vertex correspondence from segmented contours lines, PLoS One 9 (2014) e93747.
[8] Q. Long, R. Merrifield, G.Z. Yang, X.Y. Xu, P.J. Kilner, D.N. Firmin, The influence of inflow boundary conditions on intra left ventricle flow predictions, J. Biomech. Eng. 125 (2003) 922.
[9] T.B. Le, F. Sotiropoulos, On the three-dimensional vortical structure of early diastolic flow in a patient-specific left ventricle, Eur. J. Mech. B Fluid 35 (2012) 20–24.
[10] J.H. Seo, R. Mittal, Effect of diastolic flow patterns on the function of the left ventricle, Phys. Fluids 25 (2013) 110801.
[11] B. Su, F. Kabinejadian, H.Q. Phang, G.P. Kumar, F. Cui, S. Kim, R.S. Tan, J.K.F. Hon, J.C. Allen, H.L. Leo, L. Zhong, Numerical modeling of intraventricular flow during diastole after implantation of BMHV, PLoS One 10 (2015) e0126315.
[12] B. Su, L. Zhong, X.-K. Wang, J.-M. Zhang, R.S. Tan, J.C. Allen, S.K. Tan, S. Kim, H.L. Leo, Numerical simulation of patient-specific left ventricular model with both mitral and aortic valves by FSI approach, Comput. Methods Progr. Biomed. 113 (2013) 474–482.
[13] C. Chnafa, S. Mendez, F. Nicoud, Image-based large-eddy simulation in a realistic left heart, Comput. Fluids 94 (2014) 173–187.
[14] V. Vedula, R. George, L. Younes, R. Mittal, Hemodynamics in the left atrium and its effect on ventricular flow patterns, J. Biomech. Eng. 137 (2015) 1–8.
[15] S.K. Dahl, E. Thomassen, L.R. Hellevik, B. Skallerud, Impact of pulmonary venous locations on the intra-atrial flow and the mitral valve plane velocity profile, Cardiovasc. Eng. Technol. 3 (2012) 269–281.
[16] T. Doenst, K. Spiegel, M. Reik, M. Markl, J. Hennig, S. Nitzsche, F. Beyersdorf, H. Oertel, Fluid-dynamic modeling of the human left ventricle: methodology and application to surgical ventricular reconstruction, Ann. Thorac. Surg. 87 (2009) 1187–1195.
[17] J. Lantz, V. Gupta, L. Henriksson, M. Karlsson, A. Persson, C.-J. Carlhäll, T. Ebbers, Impact of pulmonary venous inflow on cardiac flow simulations: comparison with in vivo 4D flow MRI, Ann. Biomed. Eng. (2018) 1–12.
[18] W. Mao, A. Caballero, R. McKay, C. Primiano, W. Sun, Fully-coupled fluid-structure interaction simulation of the aortic and mitral valves in a realistic 3D left ventricle model, PLoS One 12 (2017) 1–21.
[19] A. Fyrenius, L. Wigström, T. Ebbers, M. Karlsson, J. Engvall, A.F. Bolger, Three

dimensional flow in the human left atrium, Heart 86 (2001) 448–455.
[20] S.K. Dahl, Numerical Simulations of Blood Flow in the Left Side of the Heart, Norwegian University of Science and Technology, 2012.
[21] V. Mihalef, R.I. Ionasec, P. Sharma, B. Georgescu, I. Voigt, M. Suehling, D. Comaniciu, Patient-specific modelling of whole heart anatomy, dynamics and haemodynamics from four-dimensional cardiac CT images, Interface Focus 1 (2011) 286–296.
[22] S.K. Dahl, J. Vierendeels, J. Degroote, S. Annerel, L.R. Hellevik, B. Skallerud, FSI simulation of asymmetric mitral valve dynamics during diastolic filling, Comput. Methods Biomech. Biomed. Eng. 15 (2012) 121–130.
[23] I. Borazjani, L. Ge, F. Sotiropoulos, High-resolution fluid-structure interaction simulations of flow through a bi-leaflet mechanical heart valve in an anatomic aorta, Ann. Biomed. Eng. 38 (2010) 326–344.
[24] B. Su, J.-M. Zhang, H.C. Tang, M. Wan, C.C.W. Lim, Y. Su, X. Zhao, R.S. Tan, L. Zhong, Patient-specific blood flows and vortex formations in patients with hypertrophic cardiomyopathy using computational fluid dynamics, 2014 IEEE Conf. Biomed. Eng. Sci, 2014, pp. 276–280.
[25] S.S. Khalafvand, L. Zhong, E.Y.K. Ng, Three-dimensional CFD/MRI modeling reveals that ventricular surgical restoration improves ventricular function by modifying intraventricular blood flow, Int. J. Numer. Method. Biomed. Eng. 30 (2014) 1044–1056.
[26] S.N. Doost, L. Zhong, B. Su, Y.S. Morsi, The numerical analysis of non-Newtonian blood flow in human patient-specific left ventricle, Comput. Methods Progr. Biomed. 127 (April 2016) 232–247.
[27] A.M. Bavo, A.M. Pouch, J. Degroote, J. Vierendeels, J.H. Gorman, R.C. Gorman, P. Segers, Patient-specific CFD simulation of intraventricular haemodynamics based on 3D ultrasound imaging, Biomed. Eng. Online 15 (2016) 1–15.
[28] J.H. Seo, V. Vedula, T. Abraham, A.C. Lardo, F. Dawoud, H. Luo, R. Mittal, Effect of the mitral valve on diastolic flow patterns, Phys. Fluids 26 (2014) 121901.
[29] A.M. Bavo, A.M. Pouch, J. Degroote, J. Vierendeels, J.H. Gorman, R.C. Gorman, P. Segers, Patient-specific CFD models for intraventricular flow analysis from 3D ultrasound imaging: comparison of three clinical cases, J. Biomech. 50 (2016) 144–150.
[30] M.S.M. Elbaz, E.E. Calkoen, J.J.M. Westenberg, B.P.F. Lelieveldt, A. a W. Roest, R.J. van der Geest, Vortex flow during early and late left ventricular filling in normal subjects: quantitative characterization using retrospectively-gated 4D flow cardiovascular magnetic resonance and three-dimensional vortex core analysis, J. Cardiovasc. Magn. Reson. 16 (2014) 78.
[31] Y. Dubief, F. Delcayre, On coherent-vortex identification in turbulence, J. Turbul. 1 (2000) N11.
[32] M.D. Cerqueira, N.J. Weissman, V. Dilsizian, A.K. Jacobs, S. Kaul, W.K. Laskey, D.J. Pennell, J.A. Rumberger, T. Ryan, M.S. Verani, Standardized myocardial segmentation and nomenclature for tomographic imaging of the heart, Circulation 105 (2002) 539–542.
[33] V. Vedula, S. Fortini, J.-H. Seo, G. Querzoli, R. Mittal, Computational modeling and validation of intraventricular flow in a simple model of the left ventricle, Theor. Comput. Fluid Dynam. 28 (2014) 589–604.
[34] G. Pedrizzetti, F. Domenichini, G. Tonti, On the left ventricular vortex reversal after mitral valve replacement, Ann. Biomed. Eng. 38 (2010) 769–773.
[35] T.-T. Le, J.A. Bryant, A.E. Ting, P.Y. Ho, B. Su, R.C.C. Teo, J.S.-J. Gan, Y.-C. Chung, D.P. O'Regan, S.A. Cook, C.W.-L. Chin, Assessing exercise cardiac reserve using real-time cardiovascular magnetic resonance, J. Cardiovasc. Magn. Reson. 19 (2017) 7.